Applied Energy 253 (2019) 113590

Contents lists available at ScienceDirect

Applied Energy

journal homepage: www.elsevier.com/locate/apenergy

Pore-scale and multiscale study of effects of Pt degradation on reactive transport processes in proton exchange membrane fuel cells

Ruiyuan Zhang[a], Ting Min[b], Li Chen[a,*], Qinjun Kang[c], Ya-Ling He[a], Wen-Quan Tao[a]

[a] Key Laboratory of Thermo-Fluid Science and Engineering of MOE, School of Energy and Power Engineering, Xi'an Jiaotong University, Xi'an, Shaanxi 710049, China
[b] School of Chemical Engineering and Technology, Xi'an Jiaotong University, Xi'an, Shaanxi 710049, China
[c] Computational Earth Science, EES-16, Earth and Environmental Sciences Division, Los Alamos National Laboratory, Los Alamos, NM 87544, USA

HIGHLIGHTS

- 3D porous structures of pristine and degraded catalyst layers are reconstructed.
- Pore-scale model for reactive transport processes in catalyst layers is developed.
- Effects of Pt degradation on reaction rate and transport resistance are evaluated.
- Multiscale simulation strategy is developed to assess the Pt degradation.

GRAPHICAL ABSTRACT

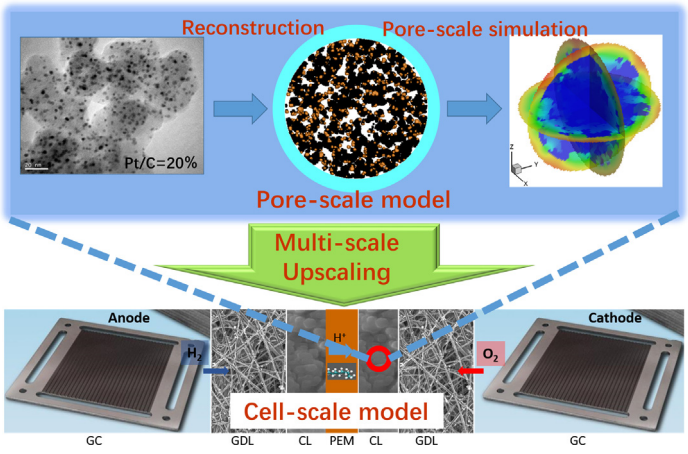

ARTICLE INFO

Keywords:
Catalyst degradation
Structure reconstruction
Catalyst layer
Pore-scale study
Lattice Boltzmann method

ABSTRACT

Understanding catalyst degradation mechanisms and their effects on reactive transport in proton exchange membrane fuel cell (PEMFC) is critical for prolonging cell lifetime. In this study, for the first time pore-scale numerical studies are conducted to explore effects of catalyst degradation on transport and electrochemical reactions in catalyst layers (CLs) of PEMFCs. High-resolution nanoscale structures of pristine and degraded CLs are reconstructed, in which detailed distributions of carbon, Pt, electrolyte and pores are resolved. Different particle size distributions of Pt agglomerates are also considered during the reconstruction. Based on the lattice Boltzmann method, pore-scale models for oxygen diffusion, interfacial dissolution, and electrochemical reaction are developed. Pore-scale modeling is then conducted to evaluate effects of Pt degradation on Pt utilization, active surface area, limiting current density and local transport resistance. It is found that total reaction rate is reduced by approximately 10–30% due to Pt degradation. Such negative effects are more prominent when Pt loading is low or more Pt is distributed in the CL interior, causing 25% and 45% increased transport resistance, respectively. Further, a multi-scale simulation strategy is proposed, and upscaling schemes for integrating pore-scale results into cell-scale models are proposed. The present study demonstrates that pore-scale simulation is a useful tool for understanding coupled mechanisms between Pt degradation and reactive transport phenomena within CLs, and is helpful for providing practical guidance for CL fabrication.

* Corresponding author.
E-mail address: lichennht08@mail.xjtu.edu.cn (L. Chen).

https://doi.org/10.1016/j.apenergy.2019.113590
Received 16 January 2019; Received in revised form 26 May 2019; Accepted 19 July 2019
Available online 01 August 2019

Nomenclature

A	total area of the reactive sites [m^2]
C	concentration [mol m^{-3}]
D	diffusivity [m^2 s^{-1}]
d	diameter of Pt particle [m]
F	Faraday's constant [C mol^{-1}]
H	Henry's constant
I_{lim}	limiting current density [A m^{-2}]
i_v	volumetric current density [A m^{-3}]
k_{elec}	reaction rate constant [m s^{-1}]
L_{CL}	CL thickness [m]
m_{Pt}	Pt loading [mg cm^{-2}]
N_{Pt}	number of Pt nodes
n_{agg}	number of agglomerates
R_{tot}	total reaction rate [mol s^{-1}]
R_{other}	gas transport resistance [s m^{-1}]
r	radius of the porous agglomerate [m]
V	volume [m^3]
$\hat{v}_{Pt}$	total volume of Pt [m^3]
x, y, z	coordinates

Greek symbols

ε_s	porosity of secondary pores
ζ_i	frequency of Pt particles in different size
ξ	ratio of the number of Pt particles inside agglomerate to the total number of Pt particles
ρ_{Pt}	density of Pt [kg m^{-3}]
ψ	total reaction rate [mol s^{-1}]
Δx	mesh size [m]

Subscripts

CL	catalyst layer
dis	dissolution reaction
eff	effective
elec	electrochemical reaction
gas	gas
N	Nafion
O_2	oxygen
Pt	platinum
s	secondary pore

1. Introduction

During the past two decades, the proton exchange membrane fuel cell (PEMFC) has drawn extensive attentions, due to its high efficiency, high power density and low pollution. It has been considered as an alternative energy devise to internal combustion engines. To date, the cost and lifetime of PEMFCs are two of the major barriers for the commercialization of PEMFCs. Many studies have been conducted to predict the lifetime of PEMFCs [1–5]. Evaluation method based on empirical formula has been developed for online forecasting of the residual cell lifetime, which takes into account environmental impact and voltage degradation rate caused by operating conditions [1]. Synthesis of prognostics guidelines also has been proposed for cell state definition, selection of lifetime prediction standards and performance evaluation [2]. Recently, deep learning method based on the recurrent neutral network also has been developed for predicting cell lifetime [3].

To prolong the lifetime of PEMFCs, it is of great importance to explore the underlying degradation mechanisms in PEMFCs, especially in catalyst layers (CLs). Reactive transport processes inside CLs play crucial roles on the performance, cost and lifetime of PEMFCs [6]. In CLs, carbon-supported Pt or Pt-alloy nanoparticles have been widely adopted to accelerate O_2 reduction reaction (ORR) and H_2 oxidation reaction (HOR) in the cathode and anode CLs, respectively. It has been found that cell performance can deteriorate rapidly due to Pt degradations, especially under dynamic operating conditions [7,8]. There have been many studies in the literature focusing on degradation of catalysts and four primary degradation mechanisms have been revealed [8]. (i) Ostwald ripening. Smaller Pt particles dissolve, generated Pt ions diffuse, and re-deposit onto large Pt particles [9,10]. (ii) Pt particle migration and agglomeration. Pt nanoparticles migrate and sinter with other Pt nanoparticles to form larger particles [11,12]. (iii) Re-precipitation. Pt dissolves into and diffuses inside the ionomer, and then precipitates to form new Pt particles in proton exchange membrane (PEM) or ionomer [9,10]. (iv) Pt particle detachment. Pt particles detach from carbon support due to carbon corrosion or other reasons [13–15].

In fact, the degradation of Pt is strongly affected by lots of factors such as composition of the support, structures of CL, Pt particle size, operating conditions, etc. In the literature, the accelerated stress tests (ASTs) technique is a commonly used strategy for studying catalyst degradation [8]. In ASTs, operating conditions of PEMFCs are simulated by sweeping the potential of the electrode in harsh conditions for a short amount of time. Thus effects of different factors could be investigated by changing simulation conditions, which really help to improve the understanding of degradation mechanisms in short simulation time. Very recently, the identical location-transmission electron microscopy (IL-TEM) technique has been developed, which allows direct comparisons of nanoscale CL structures in the same zone before and after degradation [16,17]. ASTs and IL-TEM have been combined and widely adopted to investigate degradations of CLs. To name a few, Mayrhofer et al. [17] first proposed the IL-TEM technique to observe the alternation of Pt/C structures before and after electrochemical treatment. The four degradation phenomena were successfully captured. Dubau et al. [18] adopted ASTs to investigate the degradation mechanisms of Pt/Vulcan XC72 electro-catalysts. They found that the degradation mechanisms strongly depended on the nature of the gas atmosphere and on the upper potential limit used in ASTs. Meier et al. [19] investigated the degradation behaviors of Pt/Vulcan catalyst under simulated start-stop conditions. They found different degradation mechanisms at one single catalyst location by IL-TEM, and these degradation pathways were illustrated to be strongly linked to each other. Currently, the degradation mechanisms are still poorly understood, due to the heterogeneous CL structures as well as the complicated reactive transport conditions involved.

Obviously, catalyst degradation has distinct influence on fuel cell performance, which is embodied in mass transport, electrochemical reaction, limiting current density, etc. It is thus of high interest to understand the effects of changes of carbon support and Pt distributions on reactive transport processes in CLs. To this end, numerical simulation is a powerful tool, which can provide detail distributions of important variables such as velocity, pressure, temperature, concentration, potential, reaction rate, etc. Several kinds of models at the continuum-scale have been developed for reactive transport processes in CLs, including the thin-film model, the homogeneous model and the agglomerate model. While the above continuum-scale models make certain assumptions of the realistic porous structures of CLs and thus are highly depended on averaged structural and transport properties of porous media. The recent trend of numerical study of CLs is the pore-

scale model, which directly takes into account the CL microscopic structures. As revealed by recent experimental results, local porous structures and distributions of different phases in CLs are significantly varied, and thus pore-scale model is especially suitable to study effects of such local and nanoscale variations on the cell performance. In the literature, pore-scale studies have been widely employed to investigate fluid flows, gas diffusion, electron and proton transport, and electrochemical reaction in CLs [20,21]. Wang et al. [22] conducted pore-scale simulations to investigate effects of CL microstructure on reactive transport processes. Fathi et al. [23] applied pore-scale simulations to investigate transport of liquid water and oxygen within the CLs. Kim and Pitsch [24] employed the lattice Boltzmann method (LBM) to evaluate the effective diffusivity in reconstructed CL structures. Carbon, ionomer, Pt and pore were considered in their reconstructed structures. Relationships between tortuosity and porosity were proposed based on the pore-scale results. Lange et al. [25] also reconstructed microstructures of CLs, and then pore-scale oxygen, proton transport, and electrochemical reactions within the reconstructed CL structures were studied. It was found that Knudsen diffusion plays an important role on effective diffusivity. Zheng and Kim [26] performed LBM to investigate effects of CL microstructure and water saturation on the effective diffusivity in CLs. It was found that both microstructures and water in micro-scale pores influence the diffusion pathways of oxygen and further influence the effective diffusivity. Chen et al. [27] adopted LBM to study local transport resistance across pore-ionomer interface. Effects of agglomerate size, Pt particle distribution and ionomer thickness on the local transport resistance were evaluated. Optimized CL structures were also proposed based on the pore-scale studies, in which mass transport was significantly enhanced [28].

From the above review, it can be concluded that Pt degradation will cause structures alternation of Pt/C and active surface loss, and their effects on cell performance loss can be quantitatively analyzed by pore-scale studies based on realistic porous structures of pristine and depredated CL structures. To the best of the author's knowledge, however, in the literature there has been no pore-scale numerical studies in this respect, and this is the objective of the present study. The aim of the present study is to understand the complicated reactive transport processes in evolved CL nanoscale structures and to evaluate effects of Pt degradation on the cell performance at the pore-scale.

The following paragraphs of the present study are arranged as follows. In Section 2, porous structures of pristine and degraded CLs are reconstructed, in which the detailed distributions of carbon, Pt, ionomer and pores before and after degradations are resolved. In Section 3, a pore-scale physicochemical model is developed which considers the dissolution of oxygen at pore/ionomer interface and electrochemical reactions at the reactive sites. In Section 4, effects of Pt degradation degrees, reaction rate, Pt loading, and Pt particle distributions on reactive transport processes are investigated in detail at the pore scale. In Section 5, a multi-scale simulation strategy is further proposed to upscale the pore-scale results into cell-scale models, thus fully accounting for the effects of degradation of CLs. Ultimately, in Section 6 important conclusions are drawn based on the pore-scale and multi-scale studies.

2. Reconstruction of CL structures with Pt degradation

Porous structures resolving detail distributions of each constituent in CLs are a prerequisite for subsequent pore-scale studies of reactive transport processes. Compared with experimental techniques such as FIB-SEM, Nano-CT and X-ray, computational reconstructions based on statistical algorithms have several advantages such as low cost, high efficiency, wider range of values of important structural parameters covered, and convenience for optimization of the topology and contents of the porous media. In the literature, computational reconstructions have been widely adopted to reconstruct porous structures of CLs [21,22,25,27].

Before introducing the self-developed reconstruction algorithms in this study, it is worth mentioning that the final structure of the CLs going to be reconstructed is spherical, different from most of the existing pore-scale studies in which the domain studied is usually a rectangle. This is motivated by the widely adopted agglomerate model for the CLs. The agglomerate model is the state-of-art continuum-scale model for simulating complicated reactive transport processes in CLs of PEMFCs [29]. It has been widely observed in experiments that carbon particles tend to form agglomerates with size of hundreds of nanometers [30,31]. Recognizing such structure characteristic, the agglomerate model is proposed, in which the CL is assumed to be composed of many agglomerates and each agglomerate consists of many carbon particles [32,33], as supported by the TEM image of CLs shown in Fig. 1(a). There have been different kinds of agglomerate morphology adopted in the agglomerate model, such as plate, cylinder and sphere [34], and the last one is the most widely adopted. In a spherical agglomerate model, the spherical agglomerate core is a mixture of carbon, Pt and ionomer and it is covered by a thin ionomer film (See Fig. 2) [29,35,36]. Oxygen first transports in secondary pores between agglomerates, dissolves at the pore-ionomer film interface, diffuses inside the ionomer film, and finally arrives at the agglomerate core for electrochemical reaction, as schematically shown in Fig. 2. The agglomerate model has been successfully and widely used to study multiple reactive transport processes in CLs and to optimize the structures and phase content in CLs. To name a few [37], Cetinbas et al. [35] improved the agglomerate approach with discrete catalyst particles and captured the difference of limiting current density under different Pt loadings. Xing et al. [36] developed a two-phase flow and non-isothermal agglomerate model to study how operating temperature and width ratio of channel affect cell performance. Hao et al. [37] proposed an improved agglomerate model considering the interfacial transport resistances at ionomer, water film and Pt particle surfaces, and achieved good agreement with experimental measurement. It is worth mentioning that there are a few studies arguing the existence of agglomerate model. Nevertheless, agglomerates have been widely observed

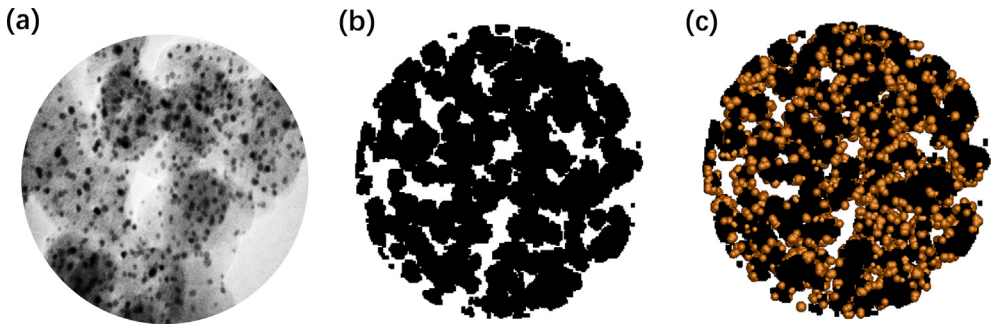

Fig. 1. Complex porous structures of CLs. (a) Microscopic structure of CL (by TEM, Pt/C = 0.2). (b) Carbon skeleton reconstructed (volume fraction of carbon is 0.4). (c) Carbon skeleton with Pt nanoparticles loaded (Pt loading = 0.2 mg cm^{-2}).

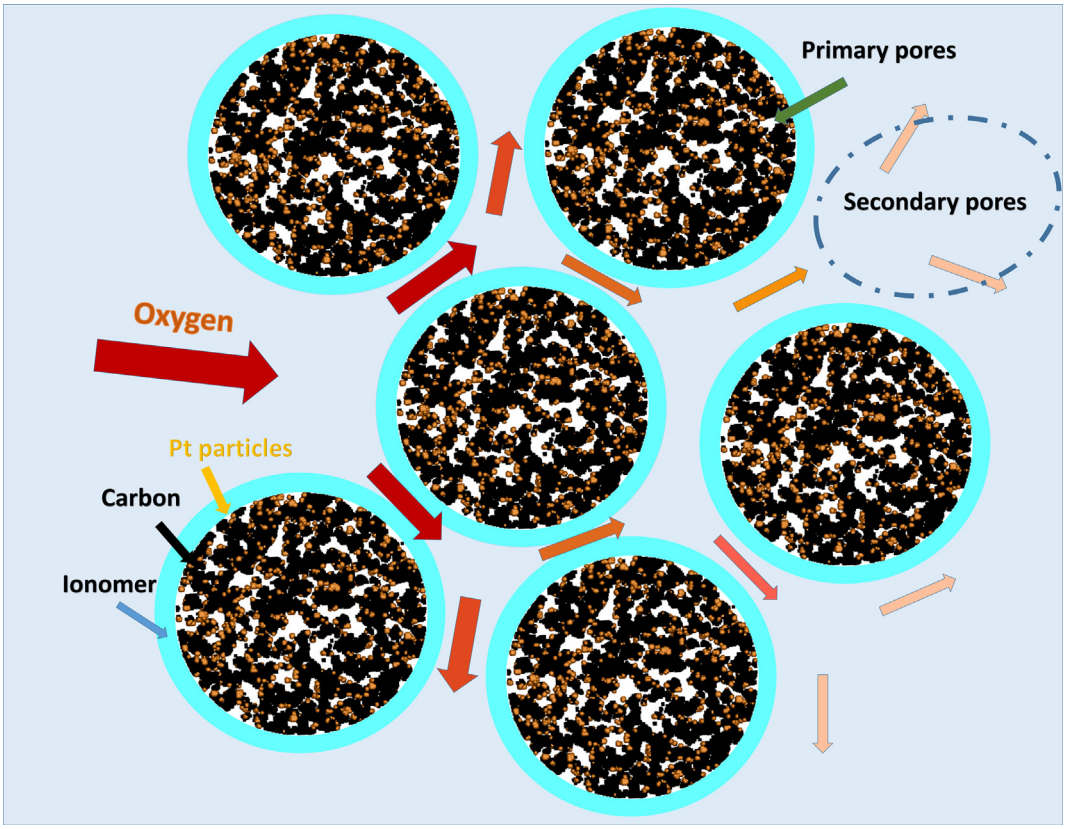

Fig. 2. Reactive transport process of oxygen between and inside the agglomerates. Oxygen transports inside the secondary pores between agglomerates, dissolves into the thin ionomer film covering the agglomerates, and reactive transport takes place inside the agglomerate cores consisted of carbon, Pt, and ionomer.

and accepted in the literature. For example, employing nano-scale resolution X-ray computed tomography (nano-CT) techniques, agglomerates with diameter from 50 to 600 nm were observed, with mean size of about 248 nm [30].

In this study, the porous CLs going to be reconstructed are similar to the above continuum-scale spherical agglomerate model. The major difference is that the homogeneous mixture assumption adopted in the agglomerate core is overcome and details of the distributions of carbon, Pt and ionomer are resolved in the pore-scale CLs. It has been proven that limiting current density predicted by continuum-scale agglomerate model is not sensitive to the Pt loading [38], and such unphysical results can be avoided by discarding the homogeneous mixture assumption adopted in the continuum-scale agglomerate models for CLs [38,39].

2.1. Reconstruction of carbon skeleton

In this study, a self-developed reconstruction algorithm is developed to reconstruct step by step each constituent in CLs. The first step is to generate the carbon skeleton by using the quartet structure generation set (QSGS) algorithm [21]. In the QSGS algorithm, firstly seeds of carbon phase are randomly distributed inside the whole spherical domain. Then, each seed is growing with a prescribed probability at each direction. Setting different values of probability along x, y and z directions can control the morphology of the carbon skeleton. In this study, the probability is the same for all the directions as the carbon particle is commonly spherical. The carbon growth process is terminated when the volume fraction of carbon phase is obtained. Details of the carbon skeleton generated are depicted in Fig. 1(b), where the volume fraction of the carbon in the domain is 40%. Compared Fig. 1(b) with Fig. 1(a), the agglomerates are well captured by the reconstruction algorithm, and complicated pore space is formed between the carbon skeletons.

2.2. Reconstruction of Pt particles

The second step of the reconstruction is to add Pt particles on the outer surface of the carbon skeleton as shown in Fig. 1(b). In fact, in the literature there have been several pore-scale studies in which details of Pt particles are considered [21,24]. In these studies, Pt particles are randomly distributed on the outer surface of the carbon support. The goal of the present study is to study effects of Pt degradation on the cell performance. Thus, nanoscale Pt degradation should be explicitly resolved in the reconstructed structures.

The self-developed algorithm for reconstructing distributions of Pt particles with different degrees of degradation contains two critical constrained parameters, the total number of Pt nodes and the particle size distributions (PSD) of Pt clusters.

The total number of Pt nodes N_{Pt} in the reconstructed domain can be calculated based on the Pt loading m_{Pt} (mg cm^{-2}) studied

$$N_{Pt} = \frac{m_{Pt}}{L_{CL}\rho_{Pt}} \frac{V_{agg}}{1-\varepsilon_s} \frac{1}{(\Delta x)^3} \quad (1)$$

where L_{CL} is the thickness of the CL, ρ_{Pt} is the density of Platinum and V_{agg} is the volume of the reconstructed domain. Note that there are two kinds of pores in the agglomerate model for CLs, the secondary pores between different agglomerates and the primary pores inside each agglomerate. ε_s in Eq. (1) is the porosity of the secondary pores. Finally, Δx in Eq. (1) is the resolution of one grid in the reconstructed structures. It is set as 2 nm in this study, which is sufficient as typical size of Pt particles is about 2 nm according to experimental observations in the literature [40].

Now attention is turned to the second constrained parameter, namely the PSD of Pt clusters. Here, a Pt cluster stands for agglomerates

of several Pt particles. In the literature, it has been widely observed that Pt particles tend to aggregate during degradation process, leading to size of Pt clusters shifting towards to larger size [8]. In this study, PSD of Pt clusters obtained from experiments in the literature is directly adopted rather than assumed. Among many experimental results in the literature, Meier's experimental results [19] are employed. Meier et al. [19] investigated the degradation of a Pt/Vulcan CL under simulated start-stop condition in a half cell. IL-TEM was adopted to directly observe changes of Pt/C structure before and after 3600 degradation cycles between 0.4 and 1.4 V at 1 V s^{-1} sweep rate. PSD of Pt clusters in the pristine and degraded CLs is provided (See Fig. 3(d) in their studies [19]), which is adopted in the present study and is plotted as S_1 and S_2 in Fig. 3. The change of PSD of Pt clusters in Ref. [19] is combined results of several Pt degradation mechanisms including Pt migration and agglomeration, Pt detachment and Ostwald ripening. Compared the two curves, it can be found that S_2, the PSD for degraded CLs, shifts towards the right side with a tail covering larger sizes. The growth of the sizes of Pt is evident. An additional curve S_3 is also studied, which is a hypothetical case related to more serious degradation situation.

Now the PSD in Fig. 3 is analyzed in detail. Fig. 3 shows the relationship between size of Pt clusters d_i and its frequency ζ_i. For a certain Pt cluster, it is represented by agglomerates of several Pt nodes in the reconstructed domain, and the number of the nodes is calculated by

$$n_{i,\mathrm{Pt}} = \frac{4}{3}\pi(0.5d_i)^3\frac{1}{(\Delta x)^3} \tag{2}$$

As mentioned previously, the resolution of one grid Δx is 2 nm in this study, which thus is sufficient to capture sizes of Pt clusters shown in Fig. 3. Therefore, the total number of all the clusters N_c can be calculated based on ζ_i, $n_{i,\mathrm{Pt}}$ and N_{Pt}

$$N_c = N_{\mathrm{Pt}} \Big/ \sum_{i=1}^{m} \zeta_i n_{i,\mathrm{Pt}} \tag{3}$$

where m denotes how many sizes of Pt clusters, which is 5, 7, and 8 for S_1, S_2 and S_3 respectively, as shown in Fig. 3. As can be seen from the image inserted in Fig. 3, due to the Pt degradation, N_c greatly reduces from 2393 for S_1 to 764 for S_3.

With the two constrained parameters prescribed, reconstruction processes of the Pt distributions are as follows. Step 1: $N_C\zeta_i$ seeds of Pt clusters with size d_i are randomly and uniformly added into the domain. Each interface node between pores and carbon phases is visited, and a random number χ is generated. If χ is lower than a prescribed probability p, and the node visited is not connected to existing Pt nodes, the status of the node is changed to Pt phase and marked as a Pt seed. Step 2: growth of the Pt seed. For a seed generated in Step 1, it will grow to the objective size d_i by adding $n_{i,\mathrm{Pt}} - 1$ Pt nodes surrounding the seed. Visiting each neighboring node of a Pt seed of interest, if it corresponds to a free pore and it is not connected to other Pt clusters, it is changed to a Pt node. This process is continued until $n_{i,\mathrm{Pt}} - 1$ neighboring Pt nodes have been added. Step 3. Repeat Steps 1 and 2 until m kinds of Pt clusters are added.

Fig. 1(c) shows the final Pt/C structures generated with Pt loading as 0.2 mg cm^{-2}. The corresponding Pt/C ratio is about 0.22. It can be seen that Pt particles are randomly dispersed on the outer surface of the carbon skeleton. Fig. 4 further displays the distribution of Pt particles in the sub-domain of $220 < x < 280$, $160 < y < 200$ and $150 < z < 170$ for different PSD of Pt clusters. It can be clearly observed that as Pt degradation increases, Pt particles aggregate and form Pt clusters with larger size.

2.3. Reconstruction of electrolyte phase

The electrolyte is assumed to completely fill the remaining spaces in the reconstructed domain that are not occupied by Pt/C. Besides, a thin electrolyte film with thickness of δ is coated on the porous agglomerate model with carbon, Pt and electrolyte.

A pore-scale physicochemical model is developed to study reactive transport processes inside the above reconstructed porous agglomerate structures of CL with different degrees of Pt degradation, and it is introduced in the following section.

3. Physicochemical processes and numerical method

Critical reactive transport processes take place inside the porous structures of CLs and at the interface between different constituents inside CLs. In this study, the outer surface of the spherical porous agglomerate is the interface between secondary pores and the thin electrolyte film. The reactive transport processes of oxygen inside the porous agglomerate contain the following steps [37,41–44]: (1) oxygen dissolution at the secondary pore/ionomer interface, (2) oxygen diffusion inside the ionomer phase, and (3) oxygen depletion at the ionomer/Pt interface.

Supposing the oxygen concentration at the outer surface is C_{gas}, it undergoes a drop when transports across the pore-ionomer interface as described by the Henry's law

$$\widetilde{C}_{\mathrm{N}} = \frac{C_{\mathrm{gas}}}{H_{\mathrm{N}}} \tag{4}$$

where H_{N} is the Henry constant. Due to the limited oxygen dissolution rate k_{dis} in the Nafion, there is a dissolution resistance at the pore/ionomer interface

$$D_{\mathrm{N}}\frac{\partial C_{\mathrm{N}}}{\partial n} = -k_{\mathrm{dis}}\left(\frac{C_{\mathrm{gas}}}{H_{\mathrm{N}}} - C_{\mathrm{N}}\right) \tag{5}$$

where k_{dis} is the dissolution reaction rate constant with unit m s^{-1}. Eq. (5) indicates that the concentration flux caused by the dissolution reaction equals to the diffusion flux inside the ionomer. Therefore, the dissolution reaction causes an additional mass transport resistance, leading to lower oxygen concentration finally arrived at the reactive sites [45–48].

In the ionomer, the oxygen concentration is governed by the Fick's law

$$\nabla(D_{\mathrm{N}}\nabla C_{\mathrm{N}}) = 0 \tag{6}$$

where D_{N} denotes the oxygen diffusion coefficient in ionomer.

There are two kinds of ionomer-solid boundary nodes, the carbon-

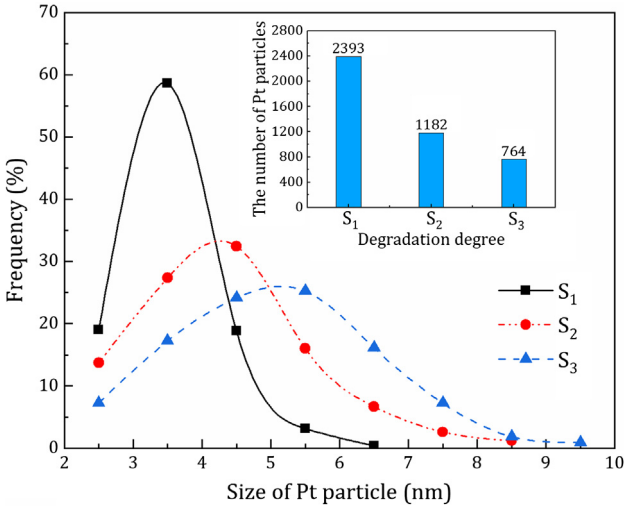

Fig. 3. Pt particle size distributions under three degrees of Pt particle degradation. The insert image shows the number of Pt particles. S_1, S_2 and S_3 represent pristine catalyst, moderate degradation and the most serious degradation in this study, respectively.

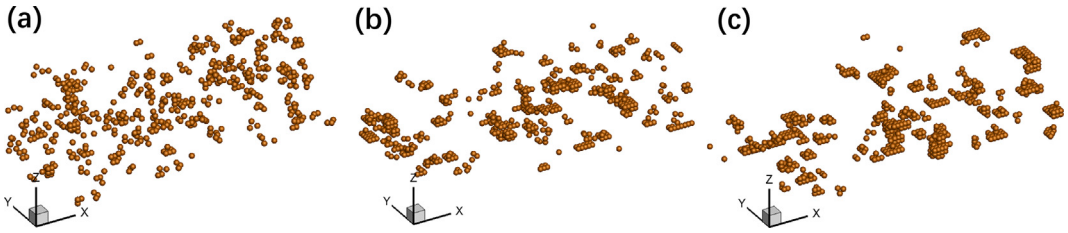

Fig. 4. Pt particle distributions under different degrees of degradation corresponding to (a) S_1, (b) S_2 and (c) S_3 in Fig. 3.

ionomer nodes and the Pt-ionomer nodes. No-flux boundary condition is adopted for the former one indicating local concentration gradient is zero. For the later one, the local electrochemical reaction is described by the Butler-Volmer equation

$$D_N \frac{\partial C_N}{\partial n} = \frac{1}{4F} \frac{C_N}{C_{O_2,ref}} i_0^{ref} \left[\exp\left(-\frac{\alpha_c F}{RT}\eta\right) - \exp\left(\frac{(1-\alpha_c)F}{RT}\eta\right)\right] = k_{elec} C_N \tag{7}$$

where F is the Faraday constant, i_0^{ref} is the exchange current density, $C_{O_2,ref}$ is the reference concentration, α_c is the transfer coefficient, R is the gas constant and T is the temperature. A lumped parameter k_{elec} adopted to denote the electrochemical reaction rate constant

$$k_{elec} = \frac{1}{4F} \frac{i_0^{ref}}{C_{O_2,ref}} \left[\exp\left(-\frac{\alpha_c F}{RT}\eta\right) - \exp\left(\frac{(1-\alpha_c)F}{RT}\eta\right)\right] \tag{8}$$

In the present study, only oxygen diffusion and electrochemical reaction are considered. Electron conduction in Pt/C and proton transfer in electrolyte are not taken into account, resulting in constant overpotential inside the entire agglomerate. This is a common assumption adopted in the continuum-scale agglomerate model in the literature, which is reasonable due to the relatively small size of the agglomerate structures studied [29].

In this work, the LBM is adopted to simulate above pore-scale oxygen reactive transport processes in the reconstructed CL structures. Due to its kinetic nature, the LBM is particularly suitable for investigating transport phenomena in porous media [49,50]. For details of the LB model for above physicochemical processes, one can refer to our previous work and it is not repeated here for the sake of brevity [27]. Table 1 lists values of important variables in the simulations.

It is worth mentioning that degradation processes of Pt particles in CLs are very complicated, which are affected by many factors such as Pt particle size, carbon support material, Pt/C structure, temperature, pressure, pH, potential, etc. Lots of studies have been devoted to this aspect to reveal the underlying mechanisms of Pt degradation under different conditions. The pore-scale model developed in this study provides a tool for evaluating the evolutions of Pt/C structures on reactive transport processes and performance of CLs. To the best of our knowledge, there has been no such study reported in the literature.

4. Results and discussion

4.1. Pt utilization and electrochemical surface area

Based on the reconstructed CL structures in Section 2, effects of Pt degradation on Pt utilization and electrochemical surface area (ECSA) are first evaluated. For all the reconstructed structures in this section, the CL agglomerate size is 160 nm, the Pt loading is 0.2 mg cm^{-2}, and the porosity inside the porous agglomerate is 0.4. Fig. 5(a) shows the distribution of Pt nodes inside the CLs, with yellow and blue nodes representing Pt nodes utilized and not utilized, respectively. Here, a Pt node can be utilized if it is exposed to the ionomer phase, namely at least one of its six neighboring nodes belonging to ionomer phase. Thus this node is accessible to oxygen for electrochemical reaction. It can be seen that as Pt degradation aggravates, the number of blue nodes increases, and blue nodes are more and more agglomerating. The Pt utilization ratio is further plotted in Fig. 5(b), which is defined as the ratio between the number of Pt nodes utilized and the total number of Pt nodes. As clearly shown in Fig. 5(b), as the Pt degradation becomes more serious, the Pt utilization ratio reduces, as expected. However, the reduce percentage is only about 4%, which is insignificant.

Fig. 5(b) further displays the variation of the ESCA. The ECSA is an important variable for evaluating the fuel cell performance, and a higher ECSA is desirable for improving cell performance. Compared with Fig. 5(b), it can be seen that reduction of the ECSA is more considerable, which is as high as 34.63%. This is explained as follows. For the Cartesian coordinates adopted in the present study, a Pt node could have six reactive surfaces at most. When Pt particle degradation takes place, reactive surfaces of a Pt particle are likely to be covered by Pt particles migrated from other sites. However, as long as one of its six reactive surfaces is not covered and is exposed to ionomer, this Pt node can still be utilized as defined previously. Therefore, the ECSA reduction is much more remarkable than the Pt utilization ratio.

As shown in Fig. 5(b), the initial ECSA of the pristine CL structure reconstructed is 94.16 $m^2 g_{Pt}^{-1}$, and after agglomerations the ECSA decreases to 61.55 $m^2 g_{Pt}^{-1}$, with a total ECSA loss of about 34.6%. In the experiments of Meier et al. [19], the ESCA was reduced from 71 $m^2 g_{Pt}^{-1}$ to 39 $m^2 g_{Pt}^{-1}$ after 3600 degradation cycles, with a total loss of about 45.1%. Note that the distributions of Pt particle size obtained experimentally by Meier et al. are adopted as the input for the reconstruction in the present study. The loss of ECSA of the present study is relatively smaller than that in Ref. [19]. This is because Pt surface oxidation is not considered during the reconstruction processes. Speder et al. [51] found the ECSA value 93.9 $m^2 g_{Pt}^{-1}$ assuming spherical Pt particles, and after ASTs the ECSA was reduced to 67.3 $m^2 g_{Pt}^{-1}$. Compared with these existing experimental results, the reconstruction method in the present study is believed to be reliable.

4.2. Total reaction rate

The ECSA loss discussed in Section 4.1 will lead to cell performance deterioration. In this section, mass transport and electrochemical reaction inside the reconstructed CLs with different degrees of degradation are studied, and the performance loss is quantitatively evaluated. The Pt loading and porosity are the same as those in Section 4.1.

Fig. 6(a) shows the oxygen concentration distribution inside the

Table 1
Structural parameters and physical properties in pore-scale simulations.

Variables	Symbol	values
Thin ionomer film thickness	δ	15 nm
Volume fraction of secondary pore	ε_s	0.5
Volume fraction of carbon in agglomerate	ε_c	0.4
Thickness of CL	L_{CL}	10 μm
Density of Pt	ρ_{Pt}	21.45 g cm^{-3}
Diffusion coefficient in ionomer	D_N	8.7×10^{-10} m^2 s^{-1}
Henry's constant in ionomer	H_N	38.9
Oxygen concentration supplied	C_0	0.8 mol m^{-3}
Lattice resolution	Δx	2 nm
Dissolution reaction rate	k_{dis}	0.00925 m s^{-1}

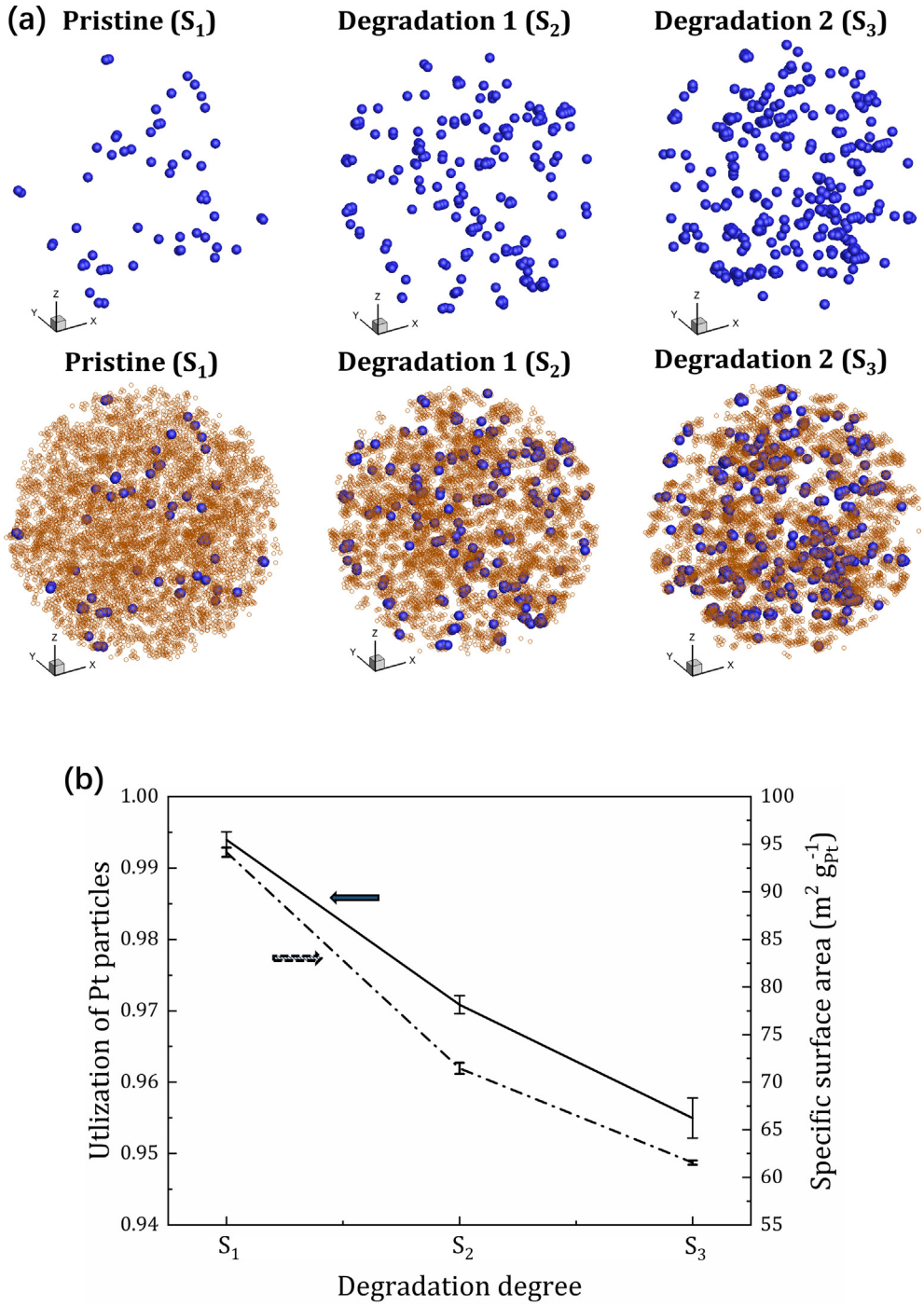

Fig. 5. Effects of Pt degradation on Pt particle distribution, Pt utilization ratio and electrochemical surface area. (a) Distributions of Pt particles with Pt loading as 0.2 mg cm^{-2}. (b) Catalyst utilization (left) and electrochemical surface area (right) both decrease with Pt degradation.

reconstructed CLs under different Damköhler numbers Da for the pristine CLs. Here, Da is a dimensionless number standing for the relative strength between chemical reaction and the diffusion process. It is defined as $k_{elec}d/D$, where k_{elec} is the electrochemical reaction rate constant of ORR defined in Eq. (8), d is the characteristic length which is the diameter of the spherical agglomerate, and D is the diffusivity of oxygen in ionomer phase. As shown in Fig. 6(a), as Da increases from 1.0×10^{-5} to 1.0×10^{5}, the penetration depth of the oxygen becomes shorter. At very high Da, the oxygen is depleted close to the periphery of the reconstructed carbon agglomerate, leading to most of the interior region starved of oxygen. The complicated concentration field is a clear indicator of the complex porous structures inside CLs and of the high transport resistance due to the tortuous void space.

Fig. 6(b) further shows effects of Pt agglomeration on the oxygen concentration field with Da as 10. It can be found that the oxygen concentration increases as Pt degradation aggravates, indicating reduced total reaction rate. This is because as Pt degradation gets serious, the number of reaction sites inside agglomerate declines, and thus less oxygen is consumed and it transports deeper into the agglomerates. Note that longer length means larger transport resistance, indicating weakening of the chemical reaction caused by the ECSA loss. This will result in reduction of the cell performance as displayed in Fig. 6(c).

Fig. 6(c) plots the relationship between Da and total reaction rate. The total reaction rate ψ is the summation of reaction rate at all the

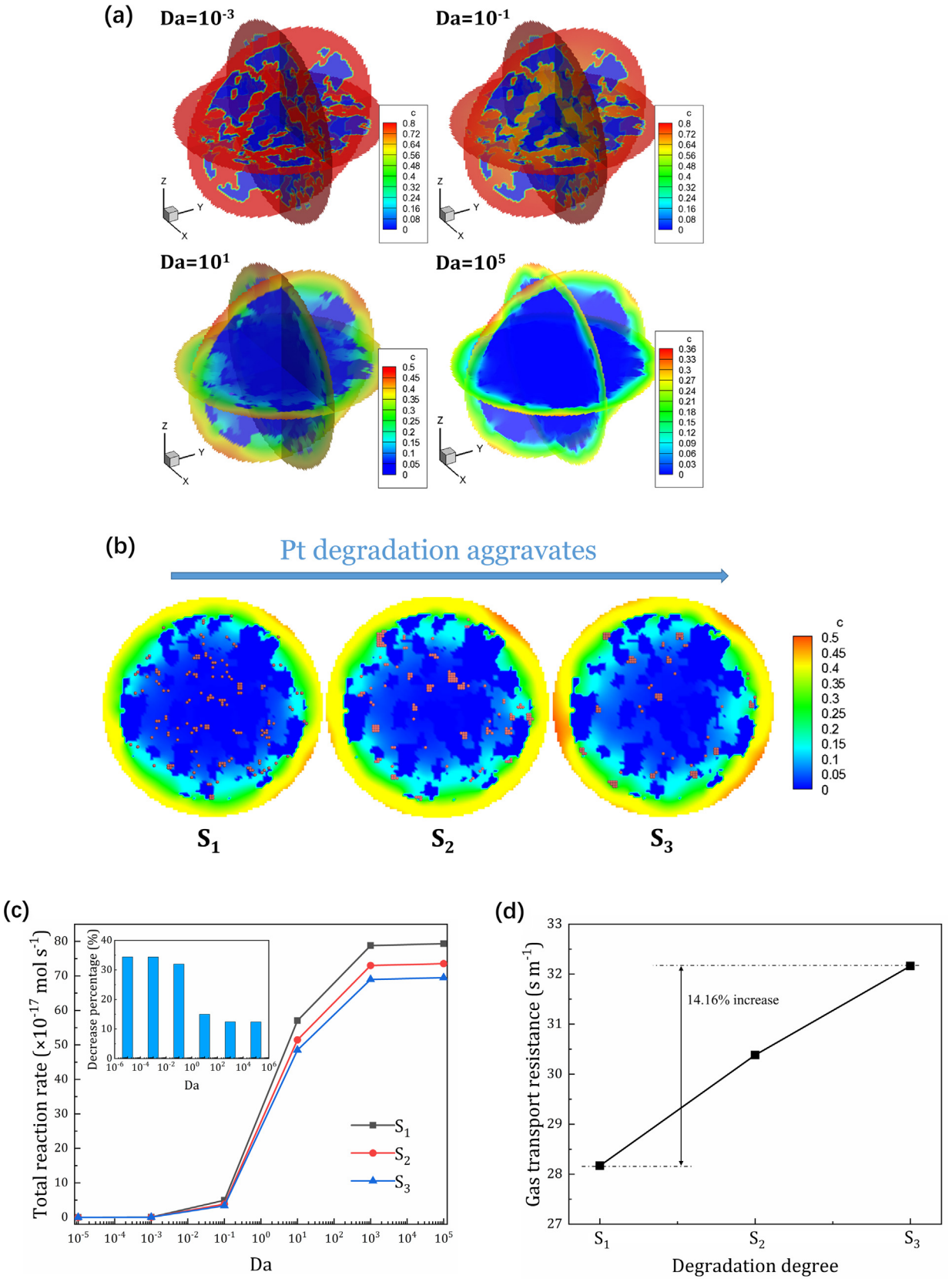

Fig. 6. Effects of Pt degradation on reactive transport in CLs. (a) 3D concentration contours under different Da numbers (S_1). (b) 2D concentration contours vary with Pt degradation (Da = 10). (c) Relationship between total reaction rate and Da. The insert image shows the decrease ratio of total reaction rate caused by Pt degradation. (d) Gas transport resistance in CLs is increased by 14.2% due to Pt degradation.

reactive sites $\sum k_{elec} C_s A$, where C_s is the surface concentration at each reaction site and A is the area of one reaction site. It can be found in Fig. 6(c) that ψ increases as Da increases, and finally approaches a constant maximum value. This maximum value corresponds to the limiting current density in a typical voltage-current density polarization curve, under which concentration polarization takes place indicating the dominant-controlled factor for the electrochemical reaction process is the slow gas diffusion. It can be observed that Pt particle degradation plays an negative effect on ψ. An interesting observation is that such negative effect is stronger under a lower Da, as indicated by the insert image in Fig. 6(c). This is explained as follows. When Da is relatively low, oxygen transports deep into the interior of the reconstructed CLs, and a relatively uniform concentration field is obtained. Under such circumstance, the ECSA loss in the entire domain plays a role on the reactive transport process. For example for Da extremely low of about 10^{-6}, the reduction of ψ from S_1 to S_3 is about 36%, almost the same as the ECSA loss shown in Fig. 5(b). However, as Da increases, more and more oxygen is consumed near the periphery of the spherical domain, and thus effects of ECSA become weaker. For example, for an extremely high Da, the performance loss is only about 10%, much smaller than the corresponding ECSA loss.

Fig. 6(d) further displays effects of Pt degradation on the local transport resistance. The oxygen transport resistance within CLs can be calculated based on the oxygen concentration obtained using limiting current density method [52]. After the simulation is converged, the maximum total reaction rate ψ_{max} is determined. Therefore, the volumetric current density i_v is calculated by

$$i_v = nF\frac{\psi_{max}}{V/(1-\varepsilon_s)} \tag{9}$$

Thus, the current density is calculated by

$$I_{lim} = i_v L_{CL} = nF\frac{\psi_{max}}{V/(1-\varepsilon_s)}L_{CL} \tag{10}$$

And the gas transport resistance in the CL is determined by

$$R_{other} = \frac{C_{gas}}{I_{lim}/nF} = \frac{C_{gas}V}{L_{CL}(1-\varepsilon_s)\psi} \tag{11}$$

As shown in Fig. 6(d), due to the ECSA loss caused by the Pt degradation, the local transport resistance increases.

4.3. Effects of Pt loading

Currently, the precious Pt accounts for a large portion of the fuel cell cost, and reducing the Pt loading is desirable for commercialization of PEMFCs. The US department of energy (DOE) sets 0.1 mg cm^{-2} as a target value by the year 2020. In this section, Pt loading from 0.05 to 0.4 mg cm^{-2} is considered, and effects of Pt degradation under different Pt loadings are explored in detail.

Fig. 7 illustrates that R_{other} increases nonlinearly as Pt loading decreases, especially when Pt loading is lower than 0.1 mg cm^{-2} the increase is dramatic, in agreement with experimental results in the literature [45,48,52]. This is because as Pt loading decreases, oxygen has to penetrate deeper into the CLs before it is completely consumed, leading to a longer diffusion length and thus higher transport resistance. In addition, it can be observed that as Pt particle degradation becomes more serious, transport resistance becomes higher, indicating reduced limiting current density. The insert image in Fig. 7 more clearly illustrates the effects of Pt particle degradation. It can be found that the increase of the transport resistance is more prominent under low Pt loading. This is due to the lower ECSA and longer diffusion length in CLs with low Pt loadings. When Pt loading is relatively low, oxygen needs to diffuse more deeply into the agglomerates before it is consumed due to insufficient reaction sites. The simulation results indicate that CLs with low Pt loading degrade more easily, raising additional challenge for enhancing durability of future PEMFCs with low Pt loading. Moreover, the pore-scale results are in acceptable agreement with the experimental results of Sakai et al. [45].

4.4. Effects of distribution location of Pt agglomerating

Up to now, in all the reconstructed CL structures Pt particles are uniformly distributed in the entire domain. In experiments, sometimes it is found that Pt particles prefer to agglomerate at certain locations. Such circumstance is thus studied in this section. The Pt loading studied is 0.1 mg cm^{-2}, and radius of carbon agglomerate is 80 nm. Separated by radius as 40 nm, carbon agglomerate is divided into two parts, the inner core region and the outside spherical ring region, as schematically shown in Fig. 8(a). Numbers of Pt particles are artificially controlled during the reconstruction processes, and a parameter ξ is introduced which is defined as the ratio of the number of Pt particles within the core region to the total number of the Pt particles. Thus, a higher ξ indicates more Pt particles are located in the interior of the reconstructed CL structures.

Fig. 8(a) shows the oxygen concentration fields under different ξ. It can be found that as ξ increases, namely more Pt particles are located inside the spherical agglomerate core region, oxygen concentration at the pore-ionomer interface becomes higher, indicating weaker chemical reaction rate inside CLs. Fig. 8(b) further displays the gas transport resistance under different ξ. It can be found that with ξ increasing from 0.2 to 0.9, R_{other} remains nearly unchanged before about 0.5 and then increases rapidly. This is because when ξ is low, there are plenty of Pt particles in the outer part of the agglomerate, providing sufficient reaction sites for the oxygen to be consumed completely. It is worth mentioning that a constant value of local transport resistance below ξ as 0.5 indicates that Pt particles inside the inner core region are actually not utilized under high current density, causing a huge waste of the precious Pt. Therefore, in order to obtain a high performance under low catalyst loading, it is highly desirable that there are sufficient catalysts restricted in the outer part, although such Pt distributions propose great challenges for the catalyst fabrication. After ξ higher than 0.5, since the volume of the outside spherical ring region is actually seven times larger than that of the inner region, Pt particles are rare in the outside region, and thus oxygen has to penetrate into the inner region as shown in Fig. 8(a), leading to higher transport resistance. Finally, it can be observed from the inset image in Fig. 8(b) that effect of Pt degradation is more prominent under a higher ξ. The results in Fig. 8 indicate that in order to alleviate effects of Pt degradation, it is highly required that the Pt particles are easier to be accessed by oxygen, which can be obtained

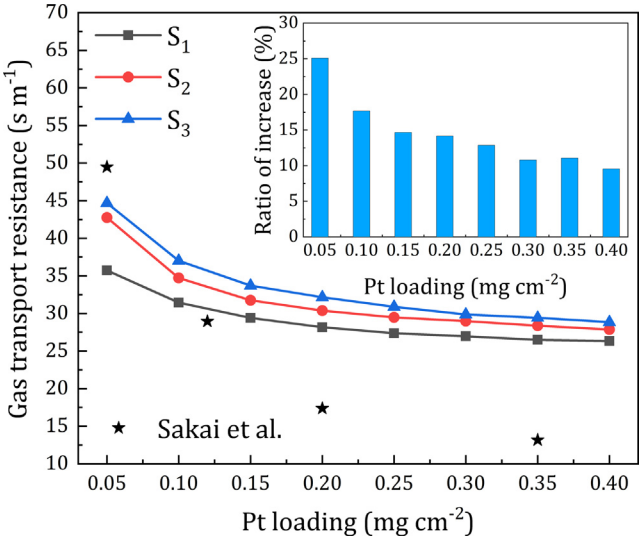

Fig. 7. Effects of Pt loading on reactive transport in CLs. The insert image shows the increase ratio of transport resistance caused by Pt degradation.

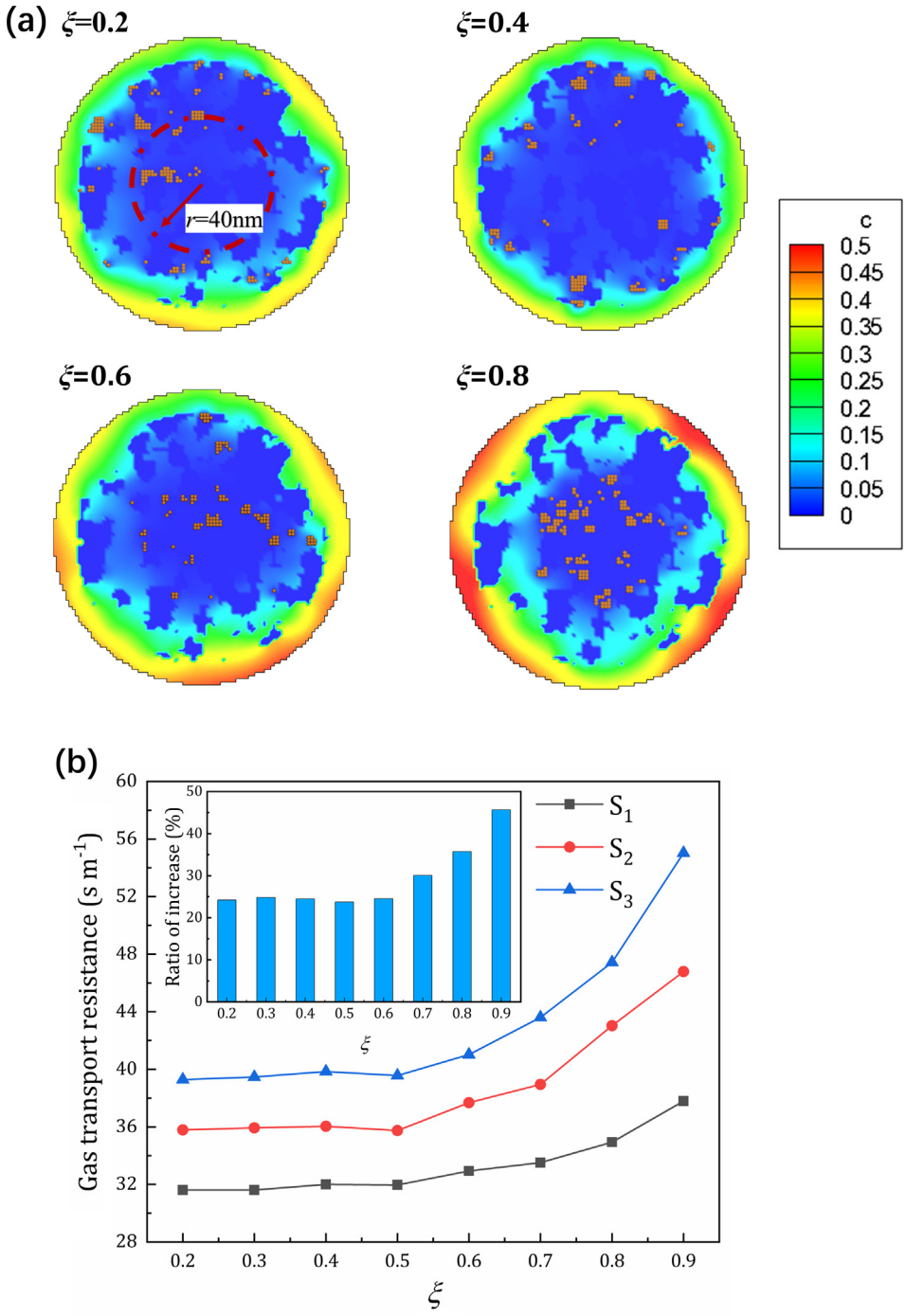

Fig. 8. Effects of Pt particle distributions on reactive transport in CLs, where ξ denotes the ratio of interior Pt particles. (a) Concentration distributions under different ξ (S_3). (b) Gas transport resistance under different ξ. The insert image describes the increase ratio of gas transport resistance caused by Pt degradation.

by distributing more Pt particles in the outside region of agglomerates as studied in this section. Reducing the agglomerate size and/or enhancing diffusivity inside the agglomerate are also helpful.

5. Multiscale numerical method

In previous sections, effects of Pt degradation on the pore-scale reactive transport processes are explored in detail. As a sub-grid model, the porous agglomerate model needs to be upscaled into cell-scale models by providing source terms to fully describe the reactive transport processes in CLs. For the continuum-scale spherical agglomerate model with homogeneous mixture assumption, there exists an analytical solution, and thus upscaling process is convenient [29]. However, the pore-scale agglomerate model is numerically solved, and the upscaling scheme from the pore-scale model to the cell-scale model should be developed and is introduced as follows.

First, sufficient pore-scale simulations are conducted to establish a database for the volumetric current density i_v under different structural and electrochemical parameters. For a given set of structure parameters of CLs, namely the agglomerate size, ionomer film thickness, and fractions of ionomer, Pt and carbon are prescribed, i_v is only a function of the overpotential η and concentration of the supplied oxygen C_{gas}. Second, based on the database provided by the first step, for intermediate values of η and C_{gas}, interpolation schemes can be employed to

obtain corresponding i_v. For the concentration, a linear interpolation scheme is sufficiently accurate. While for the overpotential, exponential interpolation scheme is recommended based on Eq. (8). Finally, i_v is employed in the cell-scale model.

To illustrate the multiscale simulation strategy, here a 1D continuum-scale CL model is combined with the pore-scale model. The governing equation for the 1D continuum-scale CL model is as follows

$$\frac{d}{dx}\left(D_{\text{eff}}\frac{dC_{\text{gas}}}{dx}\right) = \widetilde{R} \tag{12}$$

where D_{eff} represents the effective diffusivity of oxygen in CLs and is calculated by

$$D_{\text{eff}} = D\varepsilon_s^{1.5} \tag{13}$$

$\widetilde{R}$ in Eq. (12) is the source term caused by the electrochemical reaction in CLs

$$\widetilde{R} = n_{\text{agg}}\frac{i_v}{nF} \tag{14}$$

where n_{agg} is the number of CL agglomerates inside a mesh of the 1D model. The volumetric current density i_v is provided by the pore-scale simulation, and thus this source term provides the channel for exchanging information between continuum-scale and pore-scale models.

For the 1D governing equation in Eq. (12), at $x = 0$, namely the boundary between gas diffusion layer and CL, oxygen concentration is prescribed. At $x = L_{\text{CL}}$, namely the boundary between CL and proton exchange membrane, the concentration gradient is zero

$$\begin{cases} C_{\text{gas}} = C_{\text{gas}}^0 & x = 0, \text{ GDL/CL interface} \\ \frac{dC_{\text{gas}}}{dx} = 0 & x = L_{\text{CL}}, \text{ PEM/CL interface} \end{cases} \tag{15}$$

The 1D governing equation is solved using finite volume method. After the simulation convergence is obtained, the current density I (A cm^{-2}) is determined by

$$I = nF\int_0^{L_{\text{CL}}} \widetilde{R}(x)dx \tag{16}$$

Fig. 9 shows the polarization curves obtained from the multiscale simulation strategy, with pore-scale results in Fig. 6(b) adopted. The performance loss caused by Pt degradation is clearly displayed. Note that in Fig. 9 effects of Pt degradation are mainly captured in the concentration polarization region. This is because only 1D oxygen reactive transport model is considered in the present study to illustrate the implementation of multiscale simulation strategy. The extension of the current multiscale simulation strategy to the full 2D or 3D cell-scale models is straightforward, in which all the coupled reactive transport processes (oxygen transport, electron conduction, proton migration, etc.) in all components of PEMFCs (gas channel, gas diffusion layer, CL, PEM, etc.) are taken into account. Effects of Pt degradation on all the three regimes including activation, ohmic and concentration polarization regions then can be evaluated.

6. Conclusion

In this study, pore-scale numerical simulations are conducted to explore effects of Pt degradation on the reactive transport processes in CLs of PEMFCs. First, nanoscale CL structures required for subsequent pore-scale simulations are reconstructed using self-developed reconstruction algorithm. With resolution as high as 2 nm which is a typical size of Pt particles, details of distributions of carbon, Pt, electrolyte and pores are resolved. Particle size distributions of Pt for pristine and degraded CLs from experiments are also taken into account in the reconstructed CL structures.

Second, the physicochemical model for oxygen reactive transport inside CLs is introduced. The model takes into account oxygen dissolution at secondary pore-ionomer interface, oxygen diffusion inside the ionomer phase, and oxygen electrochemical reaction at the ionomer-Pt interface. Corresponding pore-scale numerical method is also developed based on the LBM.

Then, the pore-scale model is employed to study reactive transport processes inside the reconstructed CL structures with different particle size distributions of Pt representing different degrees of degradation. Effects of Pt degradation on Pt utilization, loss of ECSA, total reaction rate and local gas transport resistance are evaluated. It was found that Pt degradation leads to reduced Pt utilization and an ECSA loss as high as 34.6%. Because of the ECSA loss, total reaction rate (or current density) is also decreased, leading to higher transport resistance. Effects of Pt degradation under different Pt loading and Pt distributions are also explored, and three main conclusions are demonstrated. First, effects of Pt degradation become stronger under lower Da, caused by the longer diffusion length of oxygen before it is depleted. Compared with high Da, at low Da reaction takes place with more Pt particles, leading to greater role of ECSA loss. Second, similar with the former result, more participations in reaction of Pt particles at low Pt loading lead to greater deterioration caused by catalyst degradation. Third, more Pt distributed in interior agglomerate leads to longer path length of oxygen and greater influence of Pt degradation.

Finally, a multi-scale simulation strategy is also proposed to upscale the pore-scale results into a cell-scale model of PEMFCs. Pore-scale simulations can provide a database of volumetric current density under different overpotential and oxygen concentration. The volumetric current density is then upscaled into the cell-scale model as source terms. To illustrate the multiscale simulation strategy, a 1D continuum-scale model for CLs and pore-scale models are combined together, and negative effects of Pt degradation on cell performance are well captured in the polarization curve.

To the best of our knowledge, this is the first report that pore-scale numerical study is conducted to investigate effects of Pt degradation on reactive transport processes inside the CLs. Such study is important because it may help evaluating Pt degradation on cell performance and proposing optimized structures and operating conditions to alleviate Pt degradation. The mechanism of Pt degradation is complicated, although, the most typical phenomenon caused by Pt degradation is ECSA loss. For the first time pore-scale simulation is performed to reveal the coupling relationship between ECSA loss and performance loss. Pore-scale simulation in this study confirms that gas transport resistance is increased by Pt degradation and pore-scale structures and phase distributions greatly affect the degree of performance loss due to Pt degradation. The results reveal that cell performance loss is greater at low

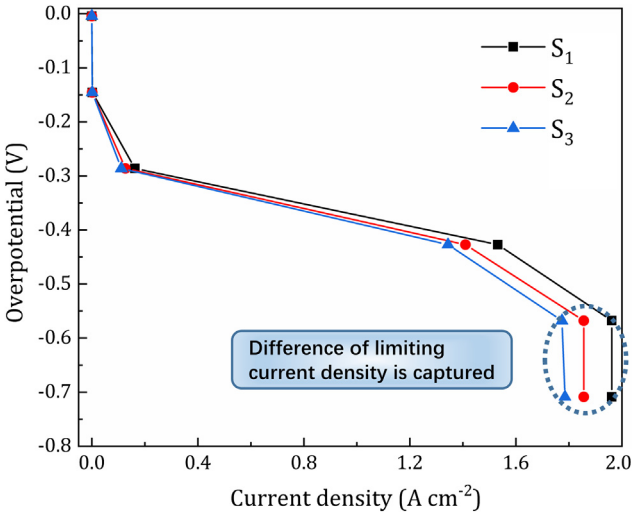

Fig. 9. Polarization curves obtained using the multiscale simulation strategy coupling continuum-scale and pore-scale CL models. S_1 to S_3 represent different degrees of Pt degradation.

Pt loading, and optimizing the Pt distributions is helpful for alleviating the effects of Pt degradation. This present study provides useful information for fabricating anti-aging CLs. It is worth mentioning that Pt degradation and reactive transport process inside CLs are in fact interacted, because on the one hand reactive transport processes cause Pt degradation, and on the other hand structural and electrochemical alternations of CLs caused by degradation change the transport and reaction processes. In the present study, structures of pristine and degraded CL structures are employed as an input for subsequent pore-scale studies of reactive transport. Coupled mechanisms between Pt degradation and reactive transport are the emphasis of future study in our group.

Acknowledgement

Li Chen thanks the support of National key research and development program (2017YFB0102702), National Nature Science Foundation of China (51776159) and Shaanxi Province Science Fund for Distinguished Young Scholars (2019JC-01).

References

[1] Chen H, Pei P, Song M. Lifetime prediction and the economic lifetime of Proton Exchange Membrane fuel cells. Appl Energy 2015;142:154–63.
[2] Jouin M, Bressel M, Morando S, Gouriveau R, Hissel D, Péra M-C, et al. Estimating the end-of-life of PEM fuel cells: guidelines and metrics. Appl Energy 2016;177:87–97.
[3] Ma R, Yang T, Breaz E, Li Z, Briois P, Gao F. Data-driven proton exchange membrane fuel cell degradation predication through deep learning method. Appl Energy 2018;231:102–15.
[4] Babu ARV, Kumar PM, Rao GS. Parametric study of the proton exchange membrane fuel cell for investigation of enhanced performance used in fuel cell vehicles. Alexandria Eng J 2018;57:3953–8.
[5] Babu ARV, Kumar PM, Rao GS. Effect of design and operating parameters on the performance of planar and ducted cathode structures of an air-breathing PEM fuel cell. Arab J Sci Eng 2016;41:3415–23.
[6] Wu H-W. A review of recent development: transport and performance modeling of PEM fuel cells. Appl Energy 2016;165:81–106.
[7] Zhang T, Wang P, Chen H, Pei P. A review of automotive proton exchange membrane fuel cell degradation under start-stop operating condition. Appl Energy 2018;223:249–62.
[8] Zhang S, Yuan X-Z, Hin JNC, Wang H, Friedrich KA, Schulze M. A review of platinum-based catalyst layer degradation in proton exchange membrane fuel cells. J Power Sources 2009;194:588–600.
[9] Borup R, Meyers J, Pivovar B, Kim YS, Mukundan R, Garland N, et al. Scientific aspects of polymer electrolyte fuel cell durability and degradation. Chem Rev 2007;107:3904–51.
[10] Shao-Horn Y, Sheng W, Chen S, Ferreira P, Holby E, Morgan D. Instability of supported platinum nanoparticles in low-temperature fuel cells. Top Catal 2007;46:285–305.
[11] Vion-Dury B, Chatenet M, Guétaz L, Maillard F. Determination of aging markers and their use as a tool to characterize Pt/C nanoparticles degradation mechanism in model PEMFC cathode environment. ECS Trans 2011;41:697–708.
[12] Meier JC, Katsounaros I, Galeano C, Bongard HJ, Topalov AA, Kostka A, et al. Stability investigations of electrocatalysts on the nanoscale. Energy Environ Sci 2012;5:9319–30.
[13] Guilminot E, Corcella A, Chatenet M, Maillard F, Charlot F, Berthomé G, et al. Membrane and active layer degradation upon PEMFC steady-state operation I. Platinum dissolution and redistribution within the MEA. J Electrochem Soc 2007;154:B1106–14.
[14] Maass S, Finsterwalder F, Frank G, Hartmann R, Merten C. Carbon support oxidation in PEM fuel cell cathodes. J Power Sources 2008;176:444–51.
[15] Linse N, Gubler L, Scherer GG, Wokaun A. The effect of platinum on carbon corrosion behavior in polymer electrolyte fuel cells. Electrochim Acta 2011;56:7541–9.
[16] Mayrhofer KJ, Meier JC, Ashton SJ, Wiberg GK, Kraus F, Hanzlik M, et al. Fuel cell catalyst degradation on the nanoscale. Electrochem Commun 2008;10:1144–7.
[17] Mayrhofer KJ, Ashton SJ, Meier JC, Wiberg GK, Hanzlik M, Arenz M. Non-destructive transmission electron microscopy study of catalyst degradation under electrochemical treatment. J Power Sources 2008;185:734–9.
[18] Dubau L, Castanheira L, Berthomé G, Maillard F. An identical-location transmission electron microscopy study on the degradation of Pt/C nanoparticles under oxidizing, reducing and neutral atmosphere. Electrochim Acta 2013;110:273–81.
[19] Meier JC, Galeano C, Katsounaros I, Topalov AA, Kostka A, Schüth F, Mayrhofer KJ. Degradation mechanisms of Pt/C fuel cell catalysts under simulated start–stop conditions. ACS Catal 2012;2:832–43.
[20] Molaeimanesh G, Googarchin HS, Moqaddam AQ. Lattice Boltzmann simulation of proton exchange membrane fuel cells – a review on opportunities and challenges. Int J Hydrogen Energy 2016;41:22221–45.
[21] Chen L, Wu G, Holby EF, Zelenay P, Tao W-Q, Kang Q. Lattice Boltzmann pore-scale investigation of coupled physical-electrochemical processes in C/Pt and non-precious metal cathode catalyst layers in proton exchange membrane fuel cells. Electrochim Acta 2015;158:175–86.
[22] Wang G, Mukherjee PP, Wang C-Y. Direct numerical simulation (DNS) modeling of PEFC electrodes: Part I. Regular microstructure. Electrochim Acta 2006;51:3139–50.
[23] Fathi H, Raoof A, Mansouri S. Insights into the role of wettability in cathode catalyst layer of proton exchange membrane fuel cell; pore scale immiscible flow and transport processes. J Power Sources 2017;349:57–67.
[24] Kim SH, Pitsch H. Reconstruction and effective transport properties of the catalyst layer in PEM fuel cells. J Electrochem Soc 2009;156:B673–81.
[25] Lange KJ, Sui P-C, Djilali N. Pore scale simulation of transport and electrochemical reactions in reconstructed PEMFC catalyst layers. J Electrochem Soc 2010;157:B1434–42.
[26] Zheng W, Kim SH. The effects of catalyst layer microstructure and water saturation on the effective diffusivity in PEMFC. J Electrochem Soc 2018;165:F468–78.
[27] Chen L, Zhang R, He P, Kang Q, He Y-L, Tao W-Q. Nanoscale simulation of local gas transport in catalyst layers of proton exchange membrane fuel cells. J Power Sources 2018;400:114–25.
[28] Chen L, Zhang R, Min T, Kang Q, Tao W. Pore-scale study of effects of macroscopic pores and their distributions on reactive transport in hierarchical porous media. Chem Eng J 2018;349:428–37.
[29] Sun W, Peppley BA, Karan K. An improved two-dimensional agglomerate cathode model to study the influence of catalyst layer structural parameters. Electrochim Acta 2005;50:3359–74.
[30] Cetinbas FC, Ahluwalia RK, Kariuki NN, Myers DJ. Agglomerates in polymer electrolyte fuel cell electrodes: Part I. Structural characterization. J Electrochem Soc 2018;165:F1051–8.
[31] Cetinbas FC, Ahluwalia RK. Agglomerates in polymer electrolyte fuel cell electrodes: Part II. Transport characterization. J Electrochem Soc 2018;165:F1059–66.
[32] Chan S, Tun W. Catalyst layer models for proton exchange membrane fuel cells. Chem Eng Technol: Ind Chem-Plant Equip-Process Eng-Biotechnol 2001;24:51–7.
[33] Wang Q, Eikerling M, Song D, Liu Z. Structure and performance of different types of agglomerates in cathode catalyst layers of PEM fuel cells. J Electroanal Chem 2004;573:61–9.
[34] Jain P, Biegler LT, Jhon MS. Sensitivity of PEFC models to cathode layer microstructure. J Electrochem Soc 2010;157:B1222–9.
[35] Cetinbas FC, Advani SG, Prasad AK. Three dimensional proton exchange membrane fuel cell cathode model using a modified agglomerate approach based on discrete catalyst particles. J Power Sources 2014;250:110–9.
[36] Xing L, Liu X, Alaje T, Kumar R, Mamlouk M, Scott K. A two-phase flow and non-isothermal agglomerate model for a proton exchange membrane (PEM) fuel cell. Energy 2014;73:618–34.
[37] Hao L, Moriyama K, Gu W, Wang C-Y. Modeling and experimental validation of Pt loading and electrode composition effects in PEM fuel cells. J Electrochem Soc 2015;162:F854–67.
[38] Cetinbas FC, Advani SG, Prasad AK. A modified agglomerate model with discrete catalyst particles for the PEM fuel cell catalyst layer. J Electrochem Soc 2013;160:F750–6.
[39] Chen L, Kang Q, Tao W. Pore-scale study of reactive transport processes in catalyst layer agglomerates of proton exchange membrane fuel cells. Electrochim Acta 2019;306:454–65.
[40] Yang Z, Ball S, Condit D, Gummalla M. Systematic study on the impact of Pt particle size and operating conditions on PEMFC cathode catalyst durability. J Electrochem Soc 2011;158:B1439–45.
[41] Kudo K, Morimoto Y. Analysis of oxygen transport resistance of Nafion thin film on Pt electrode. ECS Trans 2013;50:1487–94.
[42] Mashio T, Iden H, Ohma A, Tokumasu T. Modeling of local gas transport in catalyst layers of PEM fuel cells. J Electroanal Chem 2017;790:27–39.
[43] Moore M, Wardlaw P, Dobson P, Boisvert J, Putz A, Spiteri R, et al. Understanding the effect of kinetic and mass transport processes in cathode agglomerates. J Electrochem Soc 2014;161:E3125–37.
[44] Kudo K, Jinnouchi R, Morimoto Y. Humidity and temperature dependences of oxygen transport resistance of Nafion thin film on platinum electrode. Electrochim Acta 2016;209:682–90.
[45] Sakai K, Sato K, Mashio T, Ohma A, Yamaguchi K, Shinohara K. Analysis of reactant gas transport in catalyst layers; Effect of Pt-loadings. ECS Trans 2009;25:1193–201.
[46] Kudo K, Suzuki T, Morimoto Y. Analysis of oxygen dissolution rate from gas phase into nafion surface and development of an agglomerate model. ECS Trans 2010;33:1495–502.
[47] Greszler TA, Caulk D, Sinha P. The impact of platinum loading on oxygen transport resistance. J Electrochem Soc 2012;159:F831–40.
[48] Owejan JP, Owejan JE, Gu WB. Impact of platinum loading and catalyst layer structure on PEMFC performance. J Electrochem Soc 2013;160:F824–33.
[49] Chen L, Kang Q, Mu Y, He Y-L, Tao W-Q. A critical review of the pseudopotential multiphase lattice Boltzmann model: methods and applications. Int J Heat Mass Transf 2014;76:210–36.
[50] Chen S, Doolen GD. Lattice Boltzmann method for fluid flows. Annu Rev Fluid Mech 1998;30:329–64.
[51] Speder J, Zana A, Spanos I, Kirkensgaard JJ, Mortensen K, Hanzlik M, et al. Comparative degradation study of carbon supported proton exchange membrane fuel cell electrocatalysts–the influence of the platinum to carbon ratio on the degradation rate. J Power Sources 2014;261:14–22.
[52] Nonoyama N, Okazaki S, Weber AZ, Ikogi Y, Yoshida T. Analysis of oxygen-transport diffusion resistance in proton-exchange-membrane fuel cells. J Electrochem Soc 2011;158:B416–23.